# The Contribution of Eastern North Pacific Tropical Cyclones to the Rainfall Climatology of the Southwest United States

KRISTEN L. CORBOSIERO

*Department of Atmospheric and Oceanic Sciences, University of California, Los Angeles, Los Angeles, California*

MICHAEL J. DICKINSON

*Weather Predict Consulting, Inc., Narragansett, Rhode Island*

LANCE F. BOSART

*Department of Earth and Atmospheric Sciences, University at Albany, State University of New York, Albany, New York*

(Manuscript received 26 August 2008, in final form 6 March 2009)

ABSTRACT

Forty-six years of summer rainfall and tropical cyclone data are used to explore the role that eastern North Pacific tropical cyclones (TCs) play in the rainfall climatology of the summer monsoon over the southwestern United States. Thirty-five TCs and their remnants were found to bring significant rainfall to the region, representing less than 10% of the total number of TCs that formed within the basin. The month of September was the most common time for TC rainfall to occur in the monsoon region as midlatitude troughs become more likely to penetrate far enough south to interact with the TCs and steer them toward the north and east. On average, the contribution of TCs to the warm-season precipitation increased from east to west, accounting for less than 5% of the rainfall in New Mexico and increasing to more than 20% in southern California and northern Baja California, with individual storms accounting for as much as 95% of the summer rainfall. The distribution of rainfall for TC events over the southwest United States reveals three main categories: 1) a direct northward track from the eastern Pacific into southern California and Nevada, 2) a distinct swath northeastward from southwestern Arizona through northwestern New Mexico and into southwestern Colorado, and 3) a broad area of precipitation over the southwest United States with embedded maxima tied to terrain features. Differences in these track types relate to the phasing between, and scales of, the trough and TC, with the California track being more likely with large cutoff cyclones situated off the west coast, the southwest–northeast track being most likely with mobile midlatitude troughs moving across the intermountain west, and the broad precipitation category generally exhibiting no direct interaction with midlatitude features.

## 1. Introduction

The North American monsoon (NAM) is associated with large-scale seasonal changes in the wind and precipitation patterns over Mexico and the southwest United States [see review articles by Adams and Comrie (1997) and Higgins et al. (2003)]. Although not nearly as strong or as large as its Asian counterpart, the NAM features all of the atmospheric circulation characteristics of a classic monsoon system: 1) a reversal of the north–south temperature gradient due to strong heating of the elevated terrain of the Sierra Madre and Rocky Mountains (Li and Yanai 1996), 2) a northward shift in the axis of the subtropical ridge and westward expansion of the Bermuda high (Bryson and Lowry 1955; Carleton 1987), and 3) a reversal of the mean low-level flow over northern Mexico, the Gulf of California, and extreme southern Arizona (Badan-Dangon et al. 1991; Douglas et al. 1993; Bordoni et al. 2004).

Associated with these changes in the large-scale circulation, moisture is advected into the southwest United States northward from the Gulf of California at low levels and westward from the Gulf of Mexico at midlevels

*Corresponding author address:* Kristen L. Corbosiero, Department of Atmospheric and Oceanic Sciences, University of California, Los Angeles, 405 Hilgard Ave., Los Angeles, CA 90095.
E-mail: kristen@atmos.ucla.edu

DOI: 10.1175/2009MWR2768.1

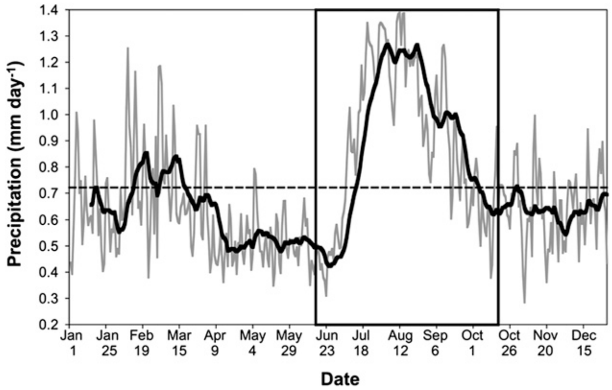


FIG. 1. Annual cycle of the average (1958–2003) daily precipitation (gray) for the southwest United States (see box in Fig. 2). The black solid curve is the 15-day running mean, the black dashed line is the daily average, and the black box defines the time period of interest for this study (16 Jun–15 Oct; i.e., the warm season).

(Rasmusson 1967; Carleton 1986; Schmitz and Mullen 1996; Higgins et al. 1997). With this influx of moisture, the precipitation (and river streamflow) over the region rapidly increases in late June, peaks in mid-August, and slowly wanes through the month of September (see Fig. 1 of Gochis et al. 2003). Figure 1, a time series of the average (1958–2003) daily precipitation over the southwest United States (see area defined in Fig. 2), shows that the daily precipitation exceeds its mean on 7 July and climbs to a peak value of nearly 1.4 mm day$^{-1}$ on 15 August before declining and falling below the mean on 27 September to give an average monsoon season length of 83 days. Note the asymmetry in the very sharp monsoon onset versus the much more gradual demise; also, the sharp increase in precipitation in late June is preceded by the climatologically driest part of the year in late May and early June.

Figure 2a shows the average warm-season (16 June–15 October) precipitation totals over the continental United States. Although the maximum rainfall amounts are confined to the eastern third of the United States (most notably over 600 mm in Florida and along the Gulf of Mexico coastline), regional maxima also appear along the low-level jet axis in the upper Midwest, along the Coast and Cascade Mountain ranges in Washington, and in conjunction with terrain features in the southwest United States including the Mogollon Rim. The contribution of these warm-season precipitation amounts to the yearly total is shown in Fig. 2b. The distribution shows minima of less than 30% over the western quarter of the United States, the lower Mississippi Valley, and the New England coastline. Relative maxima appear over Florida and along the U.S.–Canada border in the upper Midwest, with an absolute maximum in New Mexico and southeastern Arizona. With over 60% of the yearly rainfall and the strong west to east gradient in total precipitation across the southwest United States during the summer months, understanding the mechanisms that produce precipitation during the monsoon is of paramount importance for flood forecasting and water management in the region (Morehouse et al. 2000).

Because the southwest United States lies on the northern fringe of the NAM region, transient disturbances from both the tropics and midlatitudes can play a significant role in the rainfall climatology of the region (Vera et al. 2006). The most studied transient forcing mechanism for precipitation in the region is the Gulf of California moisture surge. As first discussed by Hales (1972) and Brenner (1974), the surges are accompanied by strong low-level southerly flow, higher dewpoints, cooler temperatures, and higher pressure, propagating northward along the Gulf of California. In more recent years, many observational (e.g., Fuller and Stensrud 2000; Douglas and Leal 2003; Higgins et al. 2004; Higgins and Shi 2005; Bordoni and Stevens 2006) and numerical modeling (Stensrud et al. 1997; Anderson et al. 2000a,b; Berbery and Fox-Rabinovitz 2003; Adams and Stensrud 2007) studies have documented the frequency of surge events (3–5 per month) and the percentage of monsoon season precipitation that falls on surge days (50%–100%), as well as the primary forcing mechanisms of moisture surges [i.e., tropical easterly waves or eastern North Pacific Ocean tropical cyclones (TCs) passing to the south of the Gulf of California, possibly in phase with a midlatitude trough over the northwest United States]. Half of the surges documented by Anderson et al. (2000b) and Higgins and Shi (2005) were associated with south-southeasterly flow around the eastern half of TCs in the eastern Pacific; TC-induced surges were stronger, deeper, and produced more precipitation than non-TC surges. The TCs traveled toward the northwest, past the mouth of the Gulf of California, rarely crossing 25°N before dissipating (see Fig. 1 of Higgins and Shi 2005).

Because the eastern North Pacific is climatologically the most active ocean basin for TC development (per unit area, per unit time; Molinari et al. 2000) and because TCs have been shown to play a role in transient moisture surges into the NAM region, an obvious question to ask is whether TCs themselves ever significantly impact the monsoon region. Serra (1971), Englehart and Douglas (2001), Jáuregui (2003), Larson et al. (2005), Gutzler et al. (2006), and Ritchie and Szenasi (2006) all examined the climatology and interannual variability of TCs along the western coast of Mexico and the southwest United States. Depending on the time period of study and the distance threshold

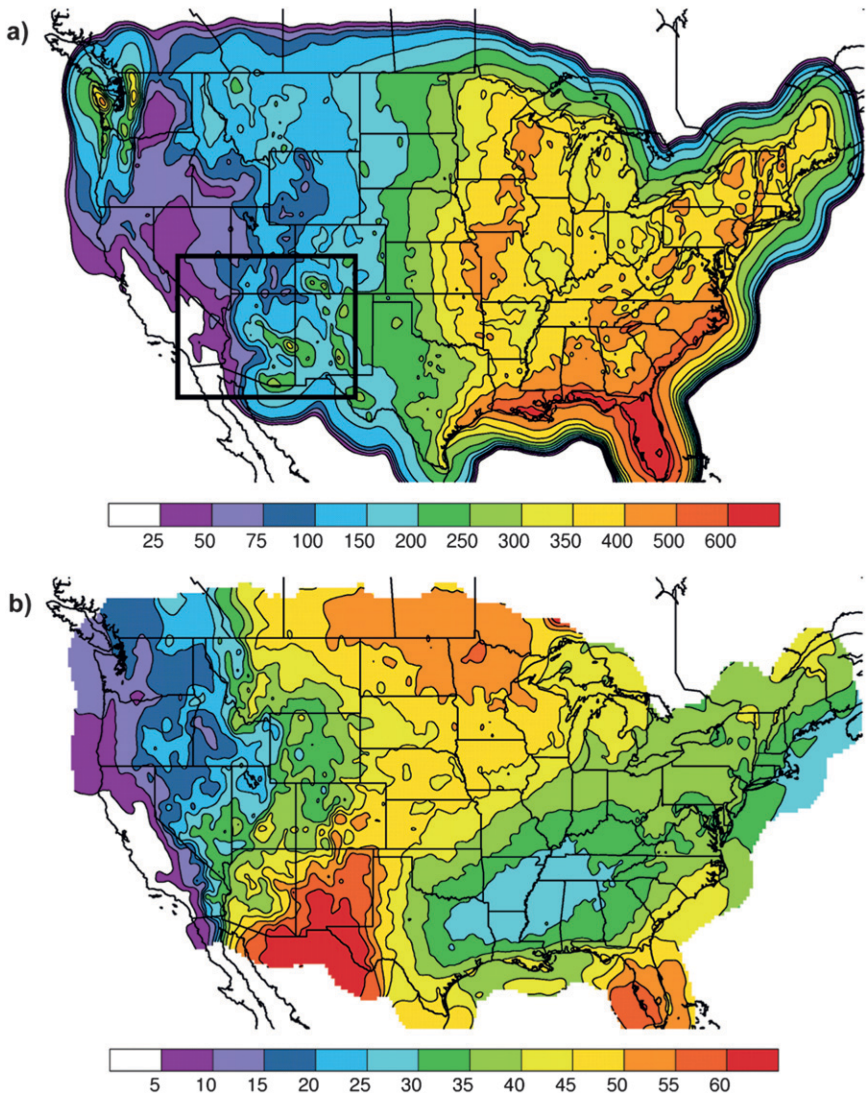


FIG. 2. Average (1958–2003) warm season (16 Jun–15 Oct) (a) total precipitation (mm) and (b) contribution to the yearly precipitation (%). The black box in (a) outlines the area 31°–40°N, 104°–118°W, defined as the southwest United States.

employed, these studies found that an average of 3–9 TCs affect western Mexico and 1–3 TCs and their remnants affect the southwest United States each year, with a maximum in the late TC season (September–November) and a signal that is modulated by the phase of El Niño–Southern Oscillation (ENSO) and the Pacific decadal oscillation. Looking at the contribution of TC rainfall in the NAM region, Englehart and Douglas (2001) noted that at least 20%–30% of the summer rain along the Mexican coast and 5%–10% in the Sierra Madre Occidental could be attributed to TCs. These values are similar to the results of Rodgers et al. (2000), who found a maximum of TC-contributed rainfall of greater than 40% just off south-central Baja California with 1%–10% over Baja, northwestern Mexico, and southern Arizona. Higher contributions of more than 20% in California with a sharp west to east gradient across the California–Arizona border were found by Larson et al. (2005), and an average of 11.4% (0%–31% range) was found by Ritchie and Szenasi (2006) over New Mexico. The dynamics of individual storms that made landfall along the Baja California and California coasts have also been extensively studied (Farfán and Zehnder 2001; Daida and Barnes 2003; Farfán 2004, 2005; Farfán and Cortez 2005) to try to understand the role of orography and midlatitude troughs in the propagation, intensity change, and precipitation structure of TCs that affect the NAM region.

The present study seeks to build on the above by addressing the contribution of eastern Pacific TCs and their remnants to the warm-season rainfall climatology of the southwest United States over a longer period of time (1958–2003), using high-resolution rainfall data and model output to construct composites and analyze case studies. Section 2 reviews the datasets and methodology used to investigate rain-producing TCs in the southwest United States, the climatology of which is presented in section 3. Section 4 examines the evolution of three representative TCs that brought rainfall to the southwest United States during the monsoon season. Finally, a summary and discussion of the results appears in section 5 with a view toward future work.

## 2. Data and methodology

The 6-hourly latitude, longitude, and intensity for each eastern Pacific TC from 16 June to 15 October 1958–2003 was obtained from the National Hurricane Center/Tropical Prediction Center (NHC/TPC) Hurricane Best Track Dataset (HURDAT). A subset of storms that crossed 25°N to the east of 130°W was chosen as a list of potential rainmakers for the southwest United States. This latitude was chosen to narrow the field of storms because it represents the southern latitude approximately 600 km from the U.S.–Mexico border. Englehart and Douglas (2001) used a similar distance of 550 km to define TC-associated rainfall in western Mexico.

Daily total precipitation was taken from the National Centers for Environmental Prediction–Climate Prediction Center (NCEP–CPC) Unified Precipitation Dataset (UPD). Over 5000 daily rainfall measurements from River Forecast Centers and the Climate Anomaly Database were used to construct the 0.25° gridded dataset that covers the region defined by 20°–60°N, 60°–140°W. (Computational details of the UPD may be found at http://www.cpc.ncep.noaa.gov/research_papers/ncep_cpc_atlas/7/toc.html.) No formal evaluation of the UPD appears in the refereed literature, but several theses conducted at the University at Albany, State University of New York (SUNY Albany), have shown that although the mesoscale details of the precipitation field (e.g., maximum amounts) are not captured, the dataset is useful for synoptic-scale interpretations such as rainfall climatologies and overall rainfall distributions of both tropical and extratropical systems (Atallah et al. 2007; Archambault et al. 2008).

Composites and standardized anomalies (relative to the 1968–96 climatological mean downloaded from http://www.cdc.noaa.gov/Composites/Day/) of the large-scale flow were calculated using the 2.5° NCEP–National Center for Atmospheric Research (NCAR) reanalysis (Kalnay et al. 1996; Kistler et al. 2001). The tracking of individual TCs and case studies employed the higher-resolution (1.125°) fields obtained from the 6-hourly 40-yr European Centre for Medium-Range Weather Forecasts (ECMWF) Re-Analysis (ERA-40; Uppala et al. 2005). The analysis of storms post-1982 was supplemented with infrared (IR) and water vapor (WV) imagery from the *Geostationary Operational Environmental Satellites* (*GOES*)*-6*, *-7*, *-9*, and *-10* [freely available from the Global International Satellite Cloud Climatology Project (ISCCP) B1 Browse System (GIBBS) online at http://www.ncdc.noaa.gov/gibbs/].

Maps of UPD rainfall were plotted for each potential rainmaking TC from the day before the TC crossed 25°N through 10 days after crossing 25°N. ERA-40 700-hPa heights and relative vorticity were used to track the storms after they weakened below tropical depression strength and/or were no longer considered tropical by NHC/TPC. The rainfall maps, together with the HURDAT and ERA-40 tracks of each storm, were then analyzed to determine on which days, if any, rainfall associated with each TC and its remnants fell in the southwest United States. For rainfall to be associated with a given storm, the system had to be deemed tropical by NHC/TPC or maintain a 700-hPa relative vorticity value of greater than $4 \times 10^{-5}\ \mathrm{s}^{-1}$ through the first day of rain in the region. It should be noted that this criterion, in addition to the storm crossing 25°N as a tropical system, eliminates a number of TCs that weakened over the eastern Pacific or that made landfall along the Mexican coast south of 25°N, whose moisture was subsequently advected into the southwest (Ritchie and Szenasi 2006), and storms that appeared to bring rainfall to the region but were not well resolved in the ERA-40 dataset [this caused the elimination of five storms between 1958 and 1971; Manning and Hart (2007) discuss the changing resolution of TCs in ERA-40]. Nonetheless, the analysis performed here revealed that 35 eastern Pacific TCs and their remnants brought rainfall to the southwest United States in the 46 yr between 1958 and 2003. Table 1 contains the list of storms, the dates they brought rainfall to the region, the states that received more than 25% of their warm-season rainfall from that TC, and the precipitation distribution category for each storm as defined in the next section.

## 3. Tropical cyclone and rainfall climatology

### *a. Storm tracks, genesis, and motion*

The NHC/TPC tracks of the 35 TCs that brought rainfall to the southwest United States are shown in Fig. 3.

TABLE 1. Eastern Pacific TCs that affected the southwest United States. The dates on which precipitation associated with the TC fell in the southwest, the precipitation distribution category (see text for definitions), and states that received greater than 25% of their warm-season (16 Jun–15 Oct) precipitation from the TC are given in the last three columns.

| Year | Storm name | Dates | Precipitation distribution category | State(s) receiving >25% of warm-season precipitation |
|---|---|---|---|---|
| 1958 | TS 10 | 10–14 Sep | SW–NE swath | AZ CO NM UT |
| | H 11 | 4–6 Oct | SW–NE swath | AZ |
| 1959 | H 10 | 11–15 Sep | CA–NV track | AZ CA NV |
| 1960 | H Diana | 19–23 Aug | Weakening in situ | AZ CO |
| 1962 | TS Claudia | 22–26 Sep | SW–NE swath | AZ CA NM NV |
| 1963 | TS Jen-Kath | 17–21 Sep | CA–NV track | AZ CA NV UT |
| 1965 | H Emily | 4–7 Sep | Weakening in situ | CA UT |
| 1966 | H Kirsten | 28 Sep–2 Oct | Weakening in situ | — |
| 1967 | H Katrina | 1–5 Sep | CA–NV track | AZ CA NV |
| 1968 | TS Hyacinth | 19–21 Aug | Weakening in situ | AZ |
| | H Pauline | 2–5 Oct | SW–NE swath | AZ CA NM UT |
| 1970 | TS Norma | 3–7 Sep | SW–NE swath | AZ CO NM UT |
| 1971 | H Olivia | 29 Sep–1 Oct | SW–NE swath | AZ CA CO NM UT |
| 1972 | H Hyacinth | 6–10 Sep | Weakening in situ | CA CO |
| | H Joanne | 5–7 Oct | SW–NE swath | AZ CA CO NM NV UT |
| 1976 | H Kathleen | 10–12 Sep | CA–NV track | AZ CA NV |
| | H Liza | 1–3 Oct | CA–NV track | NV UT |
| 1977 | H Doreen | 15–18 Aug | CA–NV track | AZ CA CO NM NV UT |
| | TS Glenda | 26–28 Sep | SW–NE swath | AZ |
| | H Heather | 6–8 Oct | Weakening in situ | AZ CA |
| 1982 | H Olivia | 24–28 Sep | CA–NV track | CA NV UT |
| 1983 | H Manuel | 18–20 Sep | Weakening in situ | CA |
| 1984 | H Marie | 9–12 Sep | Weakening in situ | AZ CA NV |
| | H Norbert | 25–27 Sep | SW–NE swath | — |
| 1986 | H Newton | 23–26 Sep | SW–NE swath | AZ CA CO NV UT |
| 1989 | H Raymond | 4–6 Oct | SW–NE swath | AZ NM |
| 1992 | H Lester | 21–25 Aug | SW–NE swath | AZ CA CO NM NV UT |
| 1993 | H Hilary | 26–30 Aug | SW–NE swath | AZ CA CO NM NV UT |
| 1995 | H Ismael | 14–16 Sep | SW–NE swath | NM |
| 1996 | H Fausto | 14–16 Sep | Weakening in situ | AZ UT |
| 1997 | H Nora | 24–27 Sep | CA–NV track | AZ CA NV |
| 1998 | H Isis | 3–7 Sep | CA–NV track | AZ CA NV UT |
| 1999 | H Hilary | 22–24 Sep | SW–NE swath | AZ CA NV |
| 2003 | H Ignacio | 26–29 Aug | Weakening in situ | AZ CA CO NM |
| | H Marty | 24–26 Sep | Weakening in situ | AZ |

The tracks in black (the storms for which precipitation plots are shown in Figs. 8 and 10) are labeled by the first letter of the storm name and year (e.g., K76 is Hurricane Kathleen 1976) at the beginning and end of the track. There is a cluster of genesis points between 10° and 15°N and centered on ~97°W, with a second larger cluster around 17°N and just west of 105°W. The storms that form farther to the south initially move just north of west before turning toward the northwest around the latitude of the northern genesis region. As required by the criterion outlined in the last section, all of the NAM region rainmakers cross 25°N as TCs (with a generally northward motion), but only slightly more than half cross 30°N, and a mere 26% have the end of their tropical tracks over the continental United States. Twenty-two TCs recurved (i.e., acquired an eastward component to their motion) and 26 storms made landfall in Baja California, western Mexico, or both, whereas only one TC in this study (TC Hyacinth 1972) made landfall solely along the U.S. coastline. Dividing the eastern Pacific HURDAT tracks into 1° × 1° grid boxes indicates that the return rate for a TC of any intensity to the U.S.–Mexico border is once every 5 yr.

To put the rare NAM region rainmaking storms in context with TC activity in the eastern Pacific as a whole, Fig. 4 shows the tracks of all TCs that formed east of 140°W and did not cross the date line from 1 August to 15 October 1958–2003. There were a total of 340 TCs during the period, meaning that just 10% of all eastern Pacific TCs and their remnants brought rainfall to the United States (the black tracks in Fig. 4). This number is not surprising considering the mean genesis position (14.4°N, 109.2°W) and motion (slightly north of due west) of all eastern Pacific storms. TCs that

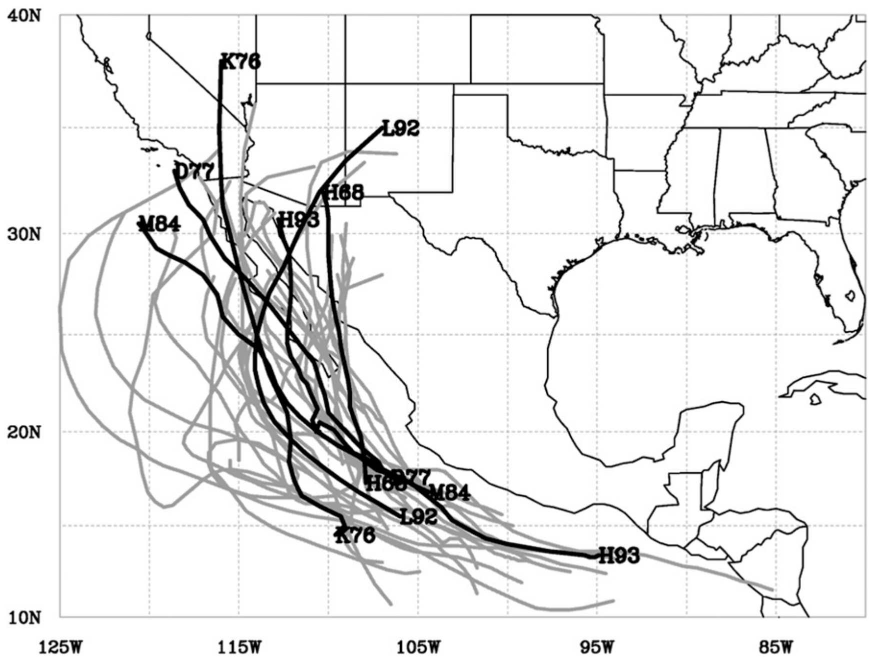


FIG. 3. NHC/TPC best tracks of the 35 eastern North Pacific tropical cyclones that affected the southwest United States. The tracks in black are the storms for which precipitation distributions are shown in Figs. 8 and 10. The tracks are labeled by the first letter of the storm's name and the last two digits of the storm's year as listed in Table 1.

eventually affect the southwest United States form ~6° farther east than the mean (significant above the 99.9% level) but only 1° farther north (significant at the 98% level). This result indicates that storms that form closer to the Mexican coast are much more likely to acquire northward and eastward components to their motion. As we shall see below, this result makes sense in the context of the large longitudinal extent of the eastern Pacific where TCs can form, but the relatively narrow latitudinal range where genesis is favored.

The main genesis region, storm motion, and sharp decrease in TCs north of 25°N can be explained by examining the climatological sea surface temperatures (SSTs), vertical wind shear, and midlevel steering flow for the month of September (the month with the highest incidence of TC rainfall; Table 1) shown in Fig. 5. Looking first at the SST pattern, the warmest waters are found immediately along the western coast of Mexico, extending north to a maximum of over 30°C in the shallow waters of the Gulf of California, and to the west with temperatures greater than 28°C in a swath between 10° and 15°N from the Mexican coastline past 130°W. SSTs decrease south of ~5°N and also along a sharp SST gradient north of 20°N and west of ~112°W. Taking into account the nominal 26.5°C for tropical cyclogenesis set forth by Gray (1968), the potential genesis area in the eastern Pacific extends from the Mexican coast westward to 130°W and beyond but is limited in the north–south direction by the cool waters of the two Pacific Ocean eastern boundary currents, California and Peru. Thus, in a climatological sense, TCs that form and track closer to the Mexican coast have a better chance of surviving the trip northward, which fits the NAM region rainmaking TC tracks that are predominantly east of 115°W (Fig. 3).

Figure 5 shows that the small latitudinal area with favorable SSTs for TC genesis is further limited at its southern edge by values of 850–200-hPa vertical wind shear exceeding 12–15 m s$^{-1}$, above which Zehr (1992) found that TCs failed to develop. This is consistent with Fig. 4, which shows that only a handful of TCs formed south of 10°N following the approximate latitude of the 12 m s$^{-1}$ shear line. As for the TCs that do develop and track toward the north and west, if the storms remain close enough to the Mexican coastline to avoid the cool SSTs from the California current, the vertical wind shear starts to increase rapidly north of ~27°N. Shear as weak as 5 m s$^{-1}$ is enough to produce a strong wavenumber-1 asymmetry in TC convection (Frank and Ritchie 1999; Corbosiero and Molinari 2002); a 10 m s$^{-1}$ shear weakened the simulated storms of Frank and Ritchie (2001) within 18–24 h of the imposition of the shear. Thus, as potential rainmaking TCs approach and cross 25°N, a combination of climatologically cool SSTs and strong

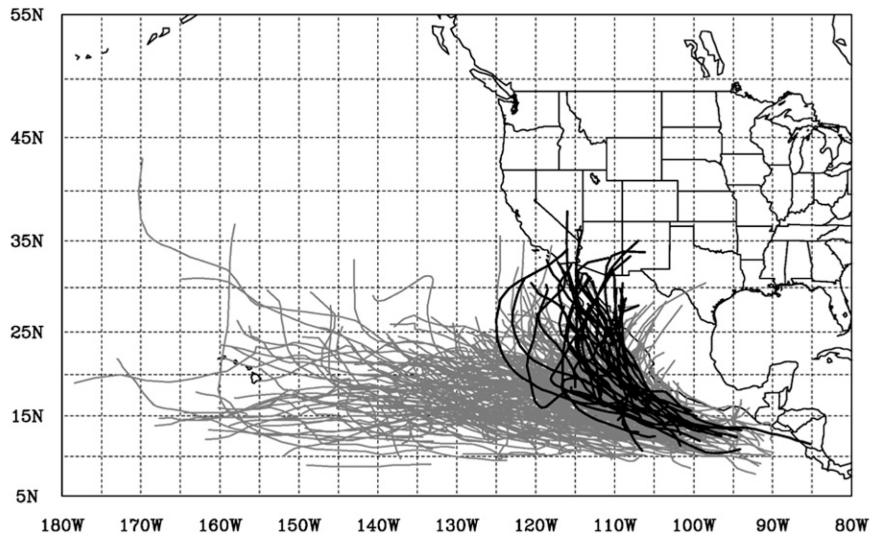


FIG. 4. NHC/TPC best tracks of all eastern North Pacific tropical cyclones that formed east of 140°W and did not cross the date line between 1 Aug and 15 Oct 1958–2003. The 35 tropical cyclones that affected the southwest United States are in black.

vertical wind shear work in concert to rapidly weaken the storms and limit their lifetimes as tropical systems.

The TCs that develop in the eastern Pacific form in a region of climatologically weak midlevel easterly flow less than 7.5 m $s^{-1}$ (black barbs in Fig. 5). Identified by Chan and Gray (1982) as the level that best correlates with the motion of TCs, the 500–700-hPa layer averaged winds are almost due east at, and south of, 15°N, only acquiring a slight northward component at 20°N. Farther north, the September climatological flow weakens further (<5 m $s^{-1}$), and turns toward the northwest and eventually north-northeast by 30°N. The motion of the 35 TCs that affected the southwest United States is generally consistent with the climatological steering flow, but with a northward component to their tracks at lower latitudes than normal and with a steeper northward component, the reasons for which will be explored in the next section.

The TCs that affect the southwest United States are unique not only in their genesis locations and storm motion but also in the time of the TC season when they are most likely to impact the region. Figure 6 shows (top) the number of days on which rainfall associated with a TC fell in the southwest United States and (bottom) the number of days at least one TC was active in the eastern Pacific. Consistent with previous studies, the most likely time for TC rainfall in the southwest United States is during the month of September. This peak in rainfall occurs during the late season secondary peak in the number of east Pacific TC days in late August and September. About equal numbers of TC rainfall days are experienced in the NAM region during the last two weeks in August and the first two weeks in October, but the number of eastern Pacific TC days in the later period is only about two-thirds of that in the earlier period. There was only one TC rainfall day during the first two weeks of August, which coincides with the midseason minimum in TC activity in the basin, consistent with the timing of the midsummer drought (Magaña et al. 1999). The peak in the eastern Pacific TC season is during the last two weeks of July, but no TCs or their remnants during the 46 yr studied impacted the southwest United States during this time. This discrepancy suggests that the large-scale flow pattern necessary to steer the storms northward is much more likely at the end of the TC season, as the atmosphere transitions to a fall pattern in the North Hemisphere.

### b. *Composite flow*

As noted in the last section, the TCs that brought rainfall to the southwest United States turned northward sooner (i.e., at lower latitudes) and with a faster speed than the climatological steering flow off the Mexican coast (Fig. 5). To investigate the reasons for this behavior, Fig. 7 shows the composite 500-hPa heights and standardized anomalies for the 20 hurricanes between 1971 and 1999 (see Table 1) to bring rainfall to the southwest United States. The composites are calculated from the NCEP–NCAR reanalysis, are relative to the day the TC crossed 25°N (day $t$), and were calculated for days $t \pm 5$, although Fig. 7 only shows days $t - 3$, $t - 1$, $t$, $t + 1$, and $t + 3$ for brevity.

On day $t - 3$ (Fig. 7a), a broad area of below-normal 500-hPa heights between 10° and 20°N and 105° to 120°W

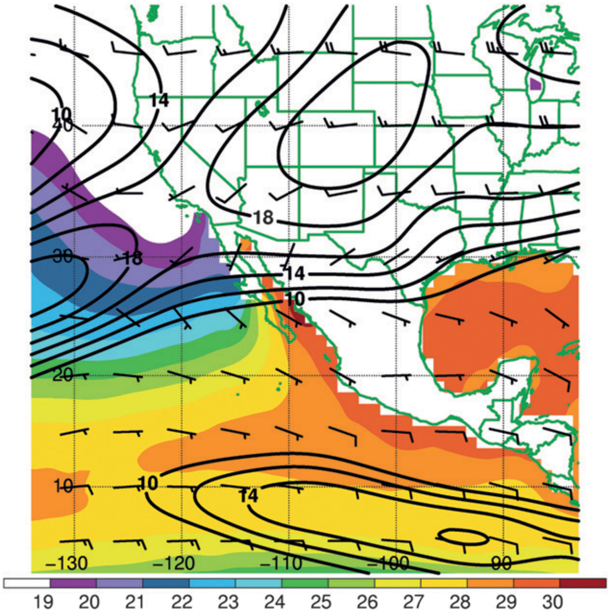


FIG. 5. Eastern North Pacific SSTs (°C; shaded), 850–200-hPa vertical wind shear (black contours every 2 m s$^{-1}$, starting at 10 m s$^{-1}$), and 500–700-hPa layer-averaged winds (black barbs, with short and long barbs indicating 2.5 and 5 m s$^{-1}$, respectively) for the month of September. The shear and layer-averaged flow are 1968–96 averages from the NCEP–NCAR reanalysis. The SST data is the 1971–2000 long-term mean from the National Oceanic and Atmospheric Administration (NOAA) optimum interpolation (OI) SST V2 dataset provided by the NOAA/Office of Oceanic and Atmospheric Research (OAR)/Earth System Research Laboratory (ESRL) Physical Sciences Division (PSD) in Boulder, CO (available on their Web site at http://www.cdc.noaa.gov/cdc/data.noaa.oisst.v2.html).

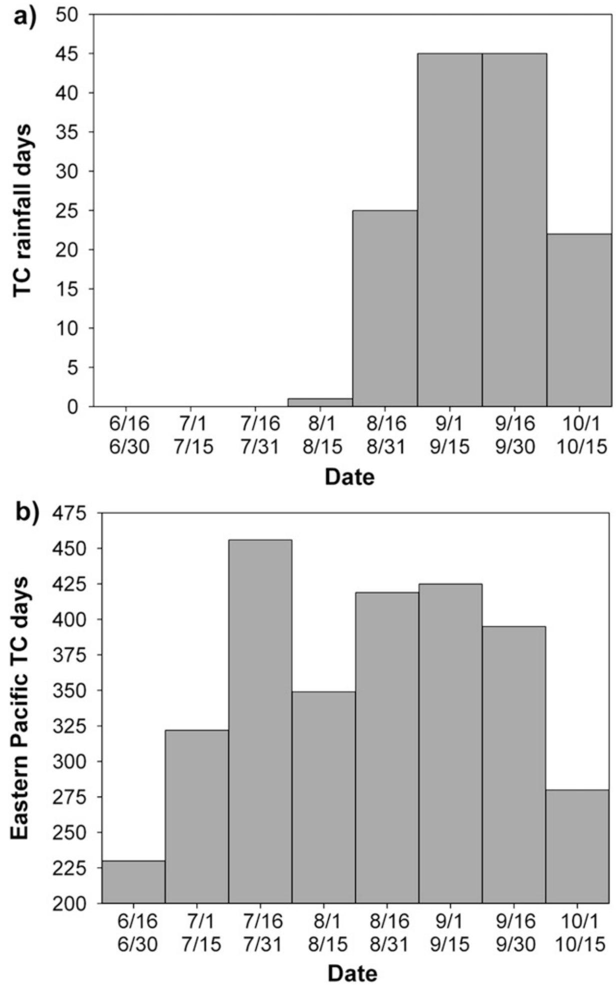


FIG. 6. Bar graphs of (a) the number of days on which rainfall from eastern North Pacific tropical cyclones fell in the southwest United States and (b) the number of days at least one tropical cyclone was active in the eastern North Pacific from 1958 to 2003.

was the NCEP–NCAR representation of the TC about to impact the southwest United States. The TC was steered toward the north around the continuous belt of high pressure to the east representing the NAM and Bermuda subtropical anticyclones. In the midlatitudes, a relatively weak trough was digging southward off the California coast, while farther north a wave train was present from just south of the Aleutian Islands across Canada and over to Greenland. Also of note on day $t - 3$ was the small patch of anomalously high heights centered on 25°N and 145°W, which increased significantly in both scale and magnitude by day $t - 1$ (Fig. 7b). An examination of the origins of these anomalously high heights in individual cases revealed influences from both convection in the central Pacific and cases of downstream development associated with the extratropical transition (ET) of western Pacific TCs. Although beyond the scope of the current study, work is presently under way to study the downstream impacts of events in the western and central Pacific on the recurvature of eastern Pacific TCs. In the current study, whatever their origin, the anomalously high heights in the composite aided in the downstream development of a deeper trough just off the California coast, a building ridge over the southern U.S. Plains, and the anomalously low heights off the southeast U.S. coast. The addition of the deeper California trough to the stationary monsoon anticyclone steered the eastern Pacific TC toward the north to a location just off Baja California on day $t - 1$. The anomaly had increased significantly in magnitude and merged with the California trough to produce one large region of below-normal heights in the eastern Pacific, with one lobe at the base of the trough and a second, stronger lobe just southwest of Baja California, representing the TC.

On day $t$ (Fig. 7c), when the TC crossed 25°N in both the HURDAT and NCEP–NCAR reanalyses, the anomaly associated with the TC was now located at the

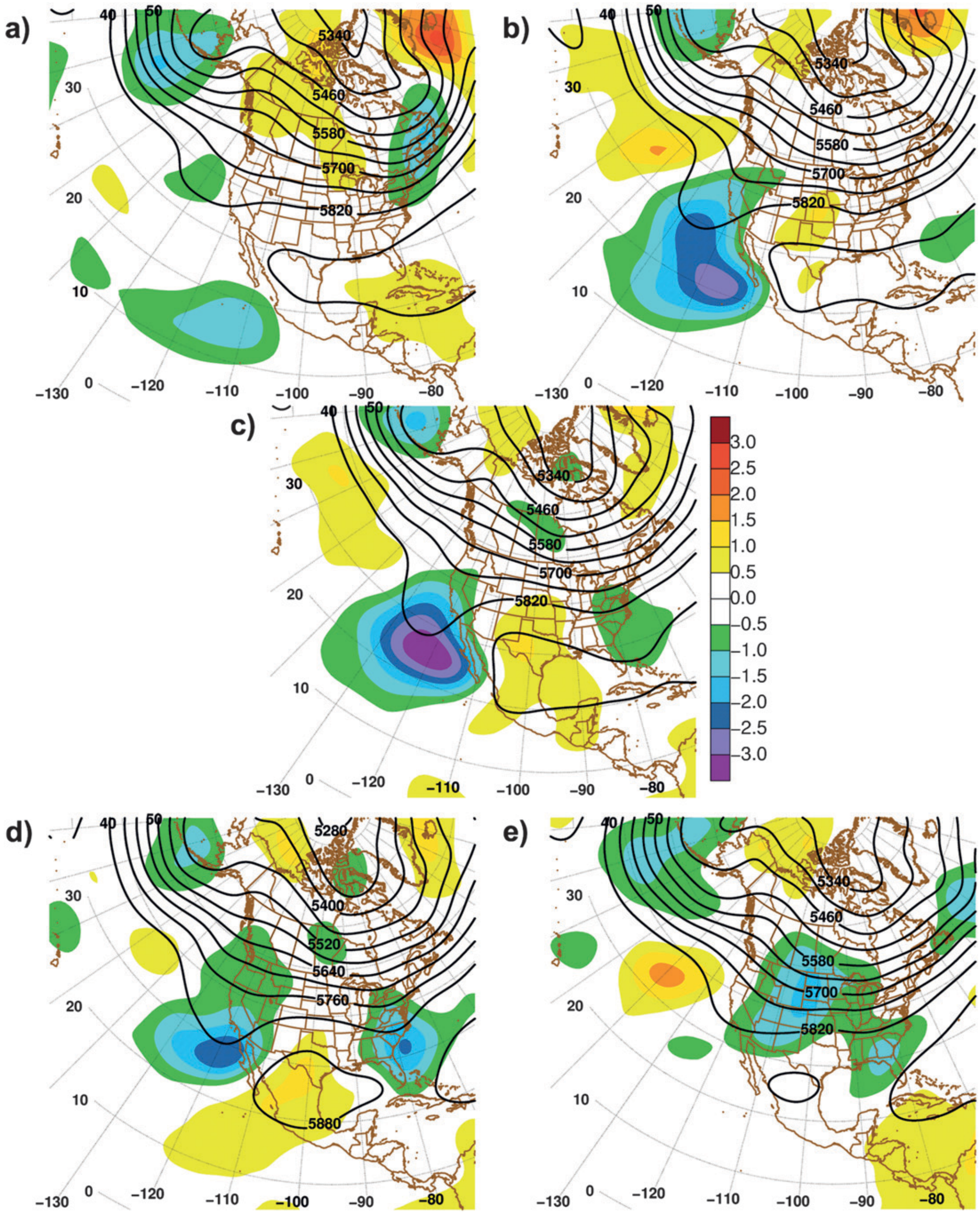


FIG. 7. Composite 500-hPa heights (m) and standardized anomalies on days (a) $t - 3$, (b) $t - 1$, (c) $t$, (d) $t + 1$, and (e) $t + 3$ for the 20 hurricanes between 1971 and 1999 to impact the southwest United States (see Table 1). Day $t$ is when the tropical cyclone crossed 25°N and anomalies are relative to the 1968–96 NCEP–NCAR reanalysis climatological mean.

base of the trough and had its largest magnitude of more than three standard deviations below the mean. At this, and subsequent times, it was no longer possible to separate the trough and the TC in the coarse reanalyses, but as we will see in the case studies below, they often remain separate entities for many days after their interaction begins. This interaction likely strengthened the downstream ridge through diabatic processes and the trough over the southeast United States through downstream development. This trough–ridge–trough pattern is similar to the 500-hPa composites for recurving eastern Pacific TCs shown by Farfán (2004) and

Ritchie and Szenasi (2006) (see Fig. 2 in each of these works) but is slightly deamplified because of the larger number of cases here versus Farfán (2004) (20 versus 6) and the inclusion of all storms, not just those with a strong trough interactions as in Ritchie and Szenasi (2006).

On day $t + 1$ (Fig. 7d), the deepening east coast trough impinged on the subtropical ridge to its south and pinched the ridge into two separate anticyclones, as the west coast trough–TC anomaly started to lift and move ashore as the anomalously high heights over the southern Plains retreated to the south. The ridge was further weakened on day $t + 3$ (Fig. 7e) as the trough–TC remnant crossed the intermountain west onto the High Plains as another strong ridge built in the eastern Pacific. The climatologically low heights over the southeast United States had weakened and retrogressed to the west on day $t + 3$, but they eventually moved slowly up the eastern seaboard in advance of the progressive Pacific trough/TC remnant (on days $t + 4$ and $t + 5$; not shown).

As will be explored below, the exact scale of and phasing between the trough and TC were different for each case and led to very different interactions, precipitation amounts, and patterns, but the features common to all events were the trough off the west coast of the United States steering the TC toward the north and the downstream ridge built by the trough–TC interaction over the continental United States.

### c. *Precipitation patterns and climatology*

The 35 TCs and their remnants that brought rainfall to the southwest United States possess a wide variety of rainfall distributions from southwest–northeast-oriented streaks extending well into the central United States to isolated pockets along the U.S.–Mexico border. The precipitation pattern depends on a number of factors including topography, the scale and nature of the west coast trough (progressive or cutoff), and the proximity of the trough to the TC. The dynamic evolution of three representative case studies will be explored in the next section, but examples of three common precipitation patterns and the average contribution of TCs to the warm-season rainfall totals over the southwest United States are presented here. (To view plots of storm total rainfall and percent contribution to the warm-season precipitation for all 35 TCs studied, see http://www.atmos.ucla.edu/~kristen/monsoon/monsoon.html.)

Figure 8 shows the storm total precipitation (mm) and the contribution of the days with TC rainfall to the warm-season precipitation (%) for Hurricane Doreen (1977), Hurricane Lester (1992), and Tropical Storm Hyacinth (1968). The warm-season contribution was simply calculated by dividing the total precipitation on days when a TC was present by the warm-season total at each grid point. As clearly evidenced by the large midlatitude trough off the California coast in the composite shown in Fig. 7, not all of the precipitation that fell on the days with a TC in the vicinity was directly associated with the TC. It is impossible, however, to separate the TC-induced rainfall from the trough-induced rainfall; thus, all rainfall that fell when a TC tracked into the NAM region will be referred to as TC rainfall.

The three storms chosen for Fig. 8 were selected because of their very different precipitation patterns and endpoints of their tropical tracks. Hurricane Doreen (1977) can be seen emerging from the tangle of tracks off Baja California around 28°N; it propagated toward the northwest, eventually weakening below tropical depression status at 0000 UTC 18 August (the end of the solid black track in Fig. 8a) just off the coast of California and below the ERA-40 relative vorticity threshold of $4 \times 10^{-5}$ s$^{-1}$ over interior southern California (the end of the dashed track) 72 h later. The precipitation pattern in Fig. 8a shows no distinct swath of heaviest rainfall and most of the local maxima are tied to the topographical features noted in the discussion of Fig. 2a. When the rainfall associated with Doreen is compared with the warm-season rainfall total, however, a different picture emerges. Because portions of southern California and Nevada typically receive less than 20 mm of rainfall during the summer (Fig. 2a), an event like Doreen accounts for greater than 50%, and in some locations 100%, of warm-season rainfall. TCs that produce their heaviest rainfall west of ~115°W and/or have the greatest contribution to the warm-season precipitation over California and Nevada will be referred to as California–Nevada track TCs. The synoptic evolution of another of the nine storms in this category (see Table 1), Hurricane Kathleen (1976), will be investigated in section 4a.

The second and largest (with 15 members; see Table 1) category of storms is called the southwest–northeast swath because of their elongated strips of heavy precipitation and long-lived vorticity maxima that strongly interact with mobile midlatitude troughs. The evolution of these storms looks most like the composite shown in Fig. 7, with the TC recurving and propagating toward the northeast in front of and along the forward edge of the trough, similar to the "full trough interaction" cases of Ritchie and Szenasi (2006). Figure 8c shows the quintessential example in this category, Hurricane Lester (1992), which produced a large swath of greater than 30 mm of rain over a 5-day period to the left of its track, covering four states from Arizona to Nebraska.

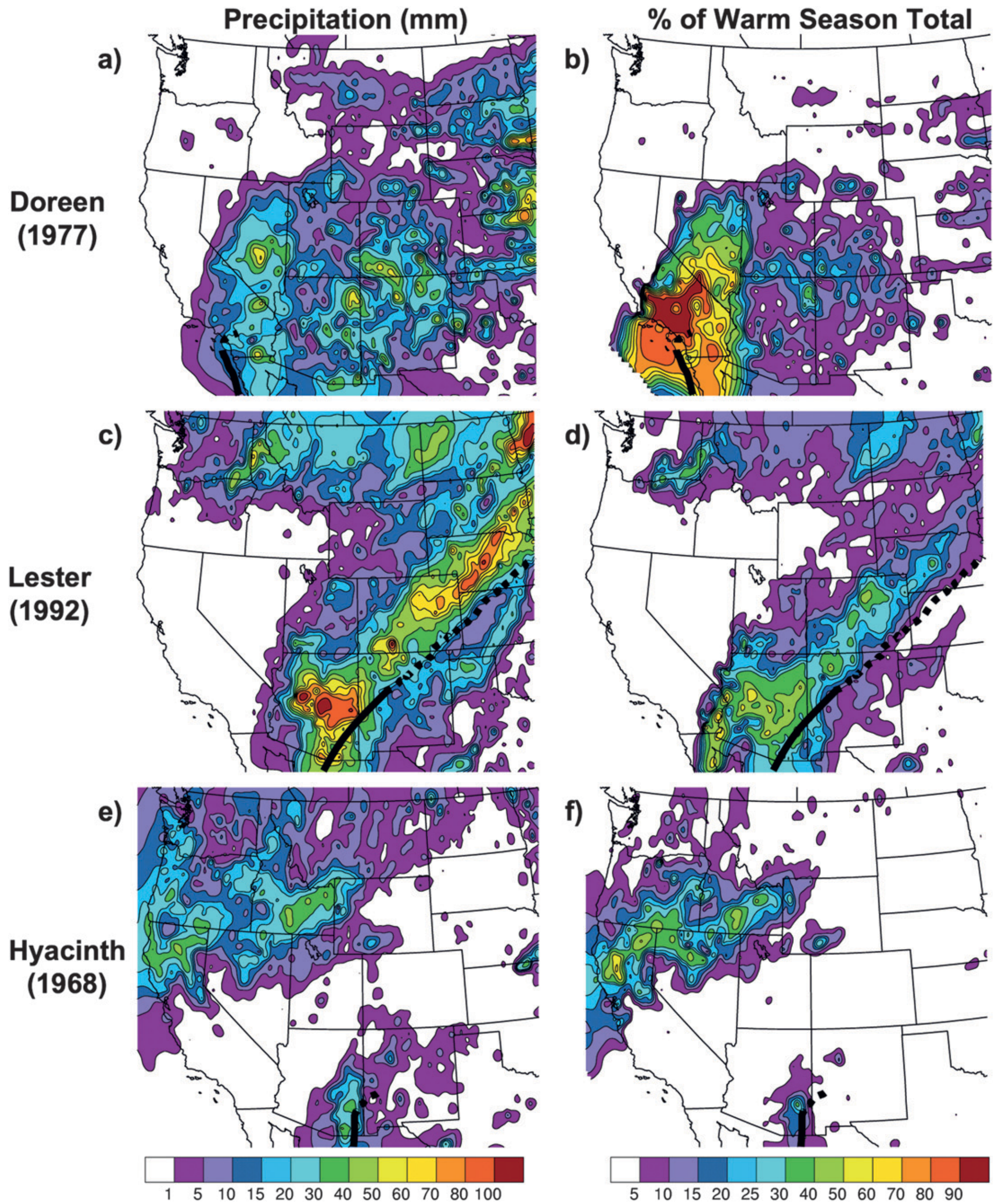


FIG. 8. (left) UPD precipitation (mm) and (right) contribution to the warm-season precipitation (%) for (top) Hurricane Doreen (15–18 Aug 1977), (middle) Hurricane Lester (21–25 Aug 1992), and (bottom) Tropical Storm Hyacinth (19–21 Aug 1968). NHC storm tracks are in solid black and ERA-40 700-hPa vorticity center tracks are dashed.

Consistent with its left of track precipitation maximum (Atallah et al. 2007), Lester has been documented to be the first case of an eastern Pacific storm to undergo ET (Dickinson et al. 2004). Because Lester will be the focus of a separate, forthcoming manuscript, the evolution of another southwest–northeast swath case, Hurricane Hilary (1993), will be explored in section 4b.

In comparison with both Doreen and Lester, the precipitation associated with Tropical Storm Hyacinth (1968) is much more isolated and confined to the end of its track along the southern Arizona–New Mexico border (Fig. 8e). A second, larger swath of precipitation associated with a midlatitude trough can be seen across the Pacific Northwest and northern

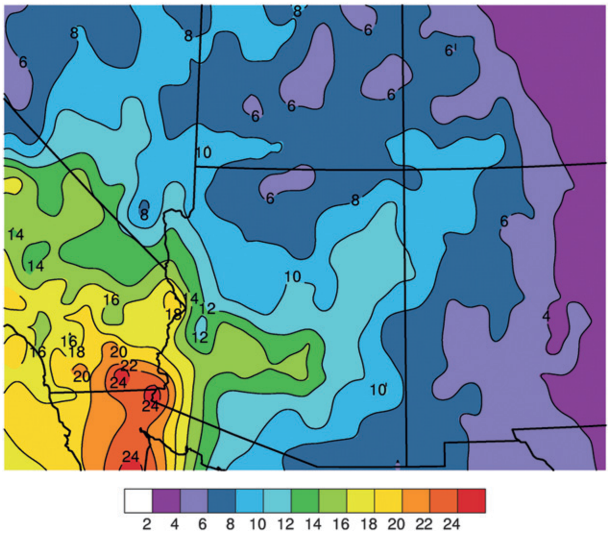


FIG. 9. Average percentage of the southwest United States warm-season (16 Jun–15 Oct) precipitation associated with eastern North Pacific tropical cyclones during the 27 yr when there was at least one tropical cyclone rainfall event in the region (see Table 1).

Rockies. In this case, the phasing between the trough and Hyacinth was such that the trough moved onshore too far north and too early to interact with Hyacinth more than steering the TC northward (analogous to the "missed interaction" category of Ritchie and Szenasi 2006). The cases that possess a missed or weak trough interaction and/or that weaken over the NAM region will be referred to as isolated or weakening in situ. Hurricane Marie (1984) will serve as an example of one of these 11 storms (see Table 1) in section 4c.

Although there are large variations in the distribution of precipitation from TCs in the southwest United States, it is useful to average the percent contribution from TC rainfall to the warm-season precipitation in the 27 yr when there was at least one TC rainfall event (see Table 1) to get a broad-brush picture of their impact on the NAM region (Fig. 9). The average contribution of TCs to the warm-season precipitation increases from east to west, accounting for less than 5% of the rainfall in eastern New Mexico and increasing to more than 20% in extreme western Arizona, southern California, and northern Baja California (similar to Fig. 2 of Larson et al. 2005). This east to west gradient is the mirror image of the gradient in average warm-season precipitation in the region (Fig. 2a), which ranges from over 200 mm in the east to less than 25 mm along the Pacific coast. Even though the plot is averaged over all 35 TCs, two of the precipitation categories defined above are evident in the percent contribution map: one extending northeast from southwest Arizona, through the northwest corner of New Mexico, and into southwestern Colorado, and the other extending north-northwest from southern to central California and into southern Nevada.

## 4. Case studies

Figure 10 shows the storm total and contribution to the warm-season precipitation for the three cases whose synoptic evolution will be examined in detail with maps of pressure on the dynamic tropopause [DT; defined as the 1.5-PVU surface (1 PVU $\equiv 10^{-6}$ m$^2$ K kg$^{-1}$ s$^{-1}$)] derived from the ERA-40 analyses. The DT was chosen over standard isobaric maps for this analysis because it provides a compact representation of the dynamically important upper-level features and because it facilitates the evaluation of the effects of diabatic heating when nonadvective rearrangement of the pressure field is present (Morgan and Nielsen-Gammon 1998). The three storms chosen for further analysis are the California–Nevada track Hurricane Kathleen (1976), the southwest–northeast swath of Hurricane Hilary (1993), and the weakening in situ Hurricane Marie (1984), shown in Figs. 10a–f, respectively. (The plots below are supplemented by higher-temporal-resolution animations for each storm at http://www.atmos.ucla.edu/~kristen/monsoon/monsoon.html.)

### *a. California–Nevada track*

Hurricane Kathleen (1976) is the eastern Pacific TC to travel the farthest north over the United States as it was tracked by NHC/TPC well into southern Nevada (Fig. 3). The storm produced in excess of 40 mm of rain over all of southern California during the 3-day period 10–12 September, which accounted for upward of 70% of the warm-season rainfall over a large portion of the region (Fig. 10b). The heaviest rainfall occurred along and to the left of the track; a distinct vorticity signature of the storm ($>4 \times 10^{-5}$ s$^{-1}$) could be tracked into southwestern Montana (Figs. 10a and 11g).

The track of Kathleen and its extremely heavy precipitation were due to the interaction of the storm with an unusually strong disturbance on the DT that fractured off of, and was left behind by, the trough located over the Dakotas at 0000 UTC 9 September (Fig. 11a). The fracture occurred 2 days earlier as the trough came ashore and the northern section continued to move steadily eastward and the cutoff disturbance sank southward and retrogressed slightly off Baja California (Figs. 11a–c). The flow around this DT disturbance steered Kathleen (labeled K in Fig. 11a) north through 1200 UTC 10 September (Fig. 11d) when it began to interact with the cyclone. The relative vorticity signature of Kathleen increased markedly to over $10 \times 10^{-5}$ s$^{-1}$ at

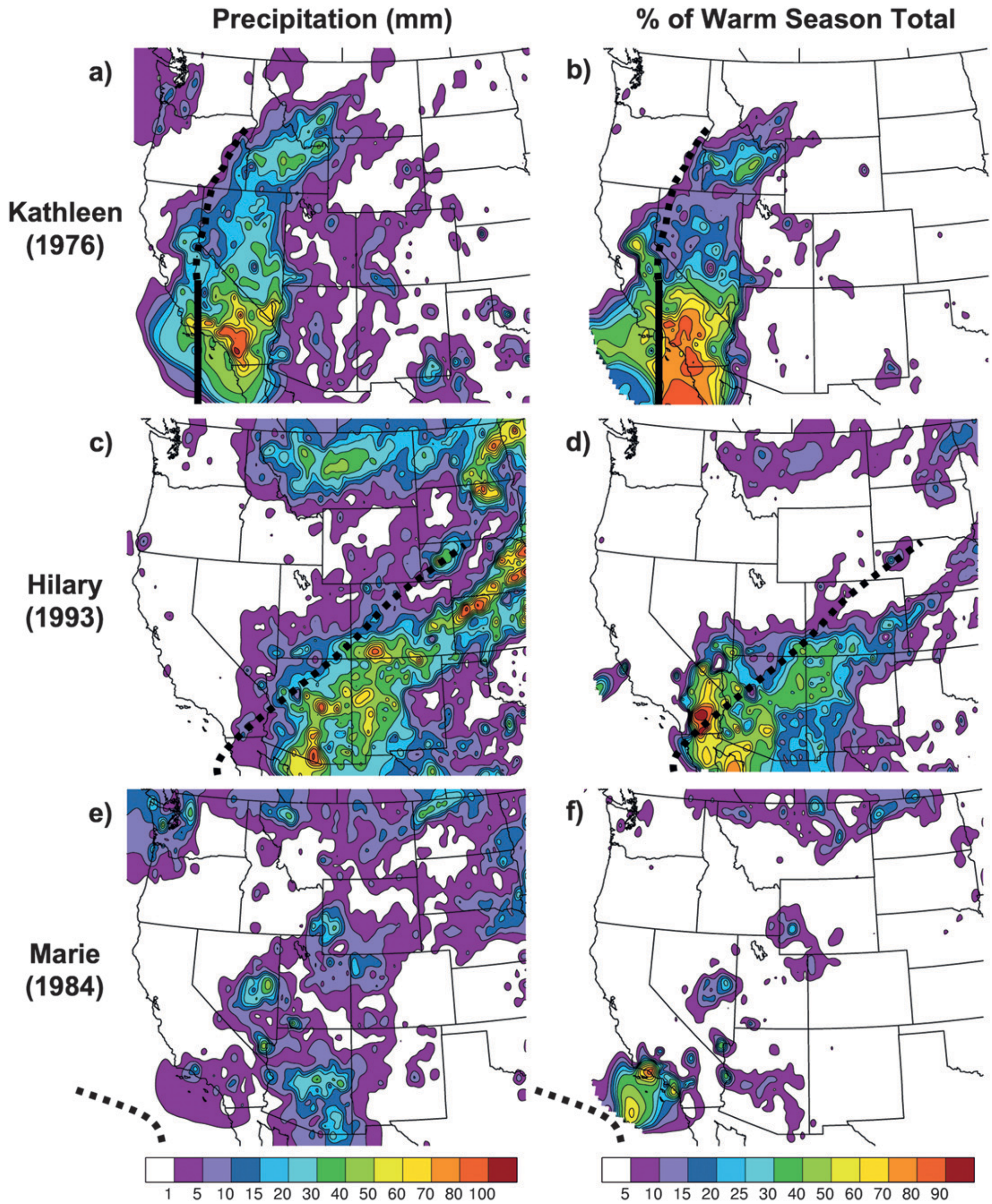


FIG. 10. As in Fig. 8, but for Hurricanes (top) Kathleen (10–12 Sep 1976), (middle) Hilary (26–30 Aug 1993), and (bottom) Marie (9–12 Sep 1984).

this time and remained stronger than any value during its time over the eastern Pacific. Although some of this increase may be due to the storm being better sampled while over the continental United States, there is undoubtedly a strong and constructive interaction between the cutoff and Kathleen, as evidenced by the left-of-track precipitation maxima (Atallah et al. 2007), the superposition of the features and kinking of the isobars on the DT in the vicinity of Kathleen, the simultaneous strengthening of the systems, and the strong downstream ridging over the southwest United States shown in Figs. 11d,e. Although no satellite imagery was available for this time period, the strong, bent-back ridge and anticyclonic outflow seen in Figs. 11d–f and the heavy precipitation amounts across the area provide strong evidence for deep convection and the diabatic generation of the ridge. The amplifying effect of downstream development in response to the southwest U.S. ridge

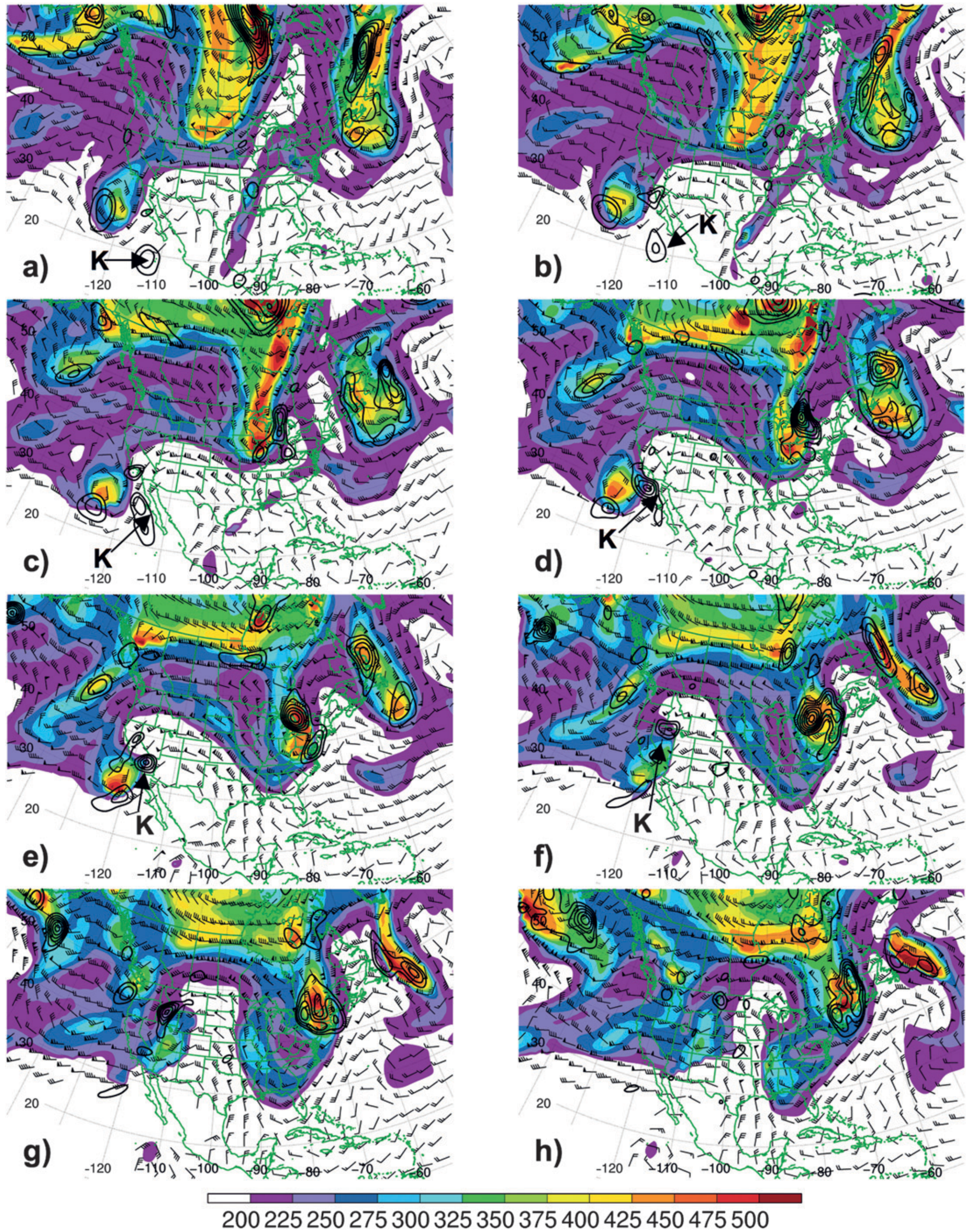


FIG. 11. Dynamic tropopause pressure (shaded every 25 hPa) and winds (barbs with short, long, and flag pennants indicating 2.5, 5, and 25 m $s^{-1}$, respectively) with 700-hPa relative vorticity (contours every $2 \times 10^{-5}$ $s^{-1}$, starting at $4 \times 10^{-5}$ $s^{-1}$). Analyses are shown every 12 h from (a) 0000 UTC 9 Sep through (h) 1200 UTC 12 Sep 1976. The NHC/TPC best track locations of Hurricane Kathleen are marked with black Ks and arrows.

eruption can be seen clearly starting on 0000 UTC 11 September and continuing through 0000 UTC 12 September (Figs. 11e–g) as the half wavelength between the ridge and downstream trough over the eastern United States contracts, a new ridge erupts over northern New England, and the next downstream trough and ridge become meridionally elongated.

Kathleen was declared extratropical by NHC at 1800 UTC 10 September and was tracked by the center for another 18 h as it cyclonically rotated around the cutoff cyclone from its eastern to northern edges. During the same time period, the cutoff began to come ashore and lift northward in response to the next upstream trough (Figs. 11d–f). As the cutoff moved ashore, it began to weaken and open up as the remnants of Kathleen weakened initially and then reintensified at 0000 UTC 12 September (Fig. 11g) before weakening again as the DT disturbance and remnants crossed the northern Rockies.

### b. *Southwest–northeast swath*

The storm total and contribution to the warm-season precipitation for Hurricane Hilary (1993) are shown in Figs. 10c,d. NHC/TPC stopped tracking Hilary south of the U.S.–Mexico border (see H93 located at ~31°N, 113°W in Fig. 2), but the TC remnants could be tracked in the ERA-40 relative vorticity field moving from southwest to northeast across central Arizona and the southern Rockies and into Nebraska (Figs. 10c and 12) during 26–30 August. Maximum precipitation values exceeding 80 mm were mostly confined to the right side of the remnant's track and contributed over 90% of the summer rainfall in southern California and over 30% along its track through Arizona and New Mexico (Fig. 10d).

The path of Hilary and its interaction with a mobile midlatitude trough can be examined through a series of daily DT and *GOES-7* WV images (at 1200 UTC) shown in Figs. 12 and 13. At 1200 UTC 23 August, Hilary was a weakening 50-kt tropical storm located southwest of the tip of Baja California (Figs. 12a and 13a). To the north of the circulation were two features of interest: 1) a strip of cyclonic shear vorticity and a relatively lower (higher pressure) DT along ~30°N that was a remnant potential vorticity streamer left behind by the trough located over the central United States, and 2) a potent midlatitude trough digging southward and coming ashore over Washington and British Columbia, seen nicely in the WV imagery in Figs. 13b,c. Over the next 48 h (Figs. 12b,c and 13b,c), Hilary slowly crept northward along the west coast of Baja California and the Pacific Northwest trough propagated south and eastward, advecting the cyclonic shear line (which had become two distinct centers by 1200 UTC 24 August in Fig. 12b) eastward and ahead of the main trough.

As the northern portion of the trough propagated quickly eastward through the northern Rockies on 26 and 27 August (Figs. 12d,e and 13d,e), the southern end of the trough thinned, became nearly stationary, and interacted with the rapidly weakening Hilary (NHC issued its last advisory for the storm at 0600 UTC 27 August). The *GOES-7* WV imagery during this period shows the deep tropical moisture associated with the remnants of Hilary streaming north and then eastward from Baja California across the Rockies and onto the central Plains in Figs. 13d–f, which likely helped build the skinny fold over the ridge (or anticyclonic wave breaking in the terminology of Thorncroft et al. 1993) spanning the upper Plains and Midwest, southern Ontario, and into New England (Fig. 12d). The remnant Hilary vorticity center, with its rich supply of tropical moisture, moved rapidly to the northeast along the front side of the weak and nearly stationary southern California trough, helping to bring over 100 mm of rain to portions of Kansas and Nebraska on 27 and 28 August. These heavy precipitation amounts continued the streak of greatest precipitation to the right of Hilary's track, consistent with the composites of Atallah et al. (2007) that showed a stronger interaction with a downstream ridge than a weak, upstream trough for recurving TCs exhibiting precipitation maxima to the right of their tracks.

### c. *Weakening in situ*

The amount and distribution of precipitation for Hurricane Marie (1984) are quite different from the two cases described above. Figure 10e reveals only isolated pockets of rainfall exceeding 30 mm in central Arizona and eastern Nevada that contribute only a small amount to the warm-season totals, except in isolated pockets on the California coast and Arizona's borders with California and Nevada (Fig. 10f). These small precipitation amounts were due to Marie's northwestward track—the first indication that it did not interact with a mobile midlatitude trough—around the western edge of an upper-level anticyclone over Mexico as seen in the DT winds at 0000 UTC 8 and 9 September in Figs. 14a,b. Ventilated by this anticyclonic flow aloft and fueled by warm waters below, Marie intensified to a strong 80-kt hurricane early on 8 September and attained an impressive satellite presentation at 0000 UTC 9 September, as seen in Fig. 15b.

As Marie moved northwestward on 9 and 10 September, the storm lost its eye and deep convection (Figs. 15c,d) as it slowly weakened to below tropical depression strength by 0000 UTC 11 September. Despite being downgraded by NHC, the Marie remnant maintained a strong relative vorticity signature exceeding $8 \times 10^{-5}\ s^{-1}$ through 0000 UTC 13 September (Fig. 14f) that can be seen in the low-level (i.e., less bright white) swirl of clouds off southern California in Figs. 15d,e. As the low-level center moved westward (see track on Fig. 10e), the moisture associated with Marie propagated to the east and help fuel afternoon convection over Arizona (Fig. 15d), which brought widespread rains of greater than 10 mm (Fig. 10e).

The strong anticyclonic circulation on the DT, originally centered east of Marie over northern Mexico

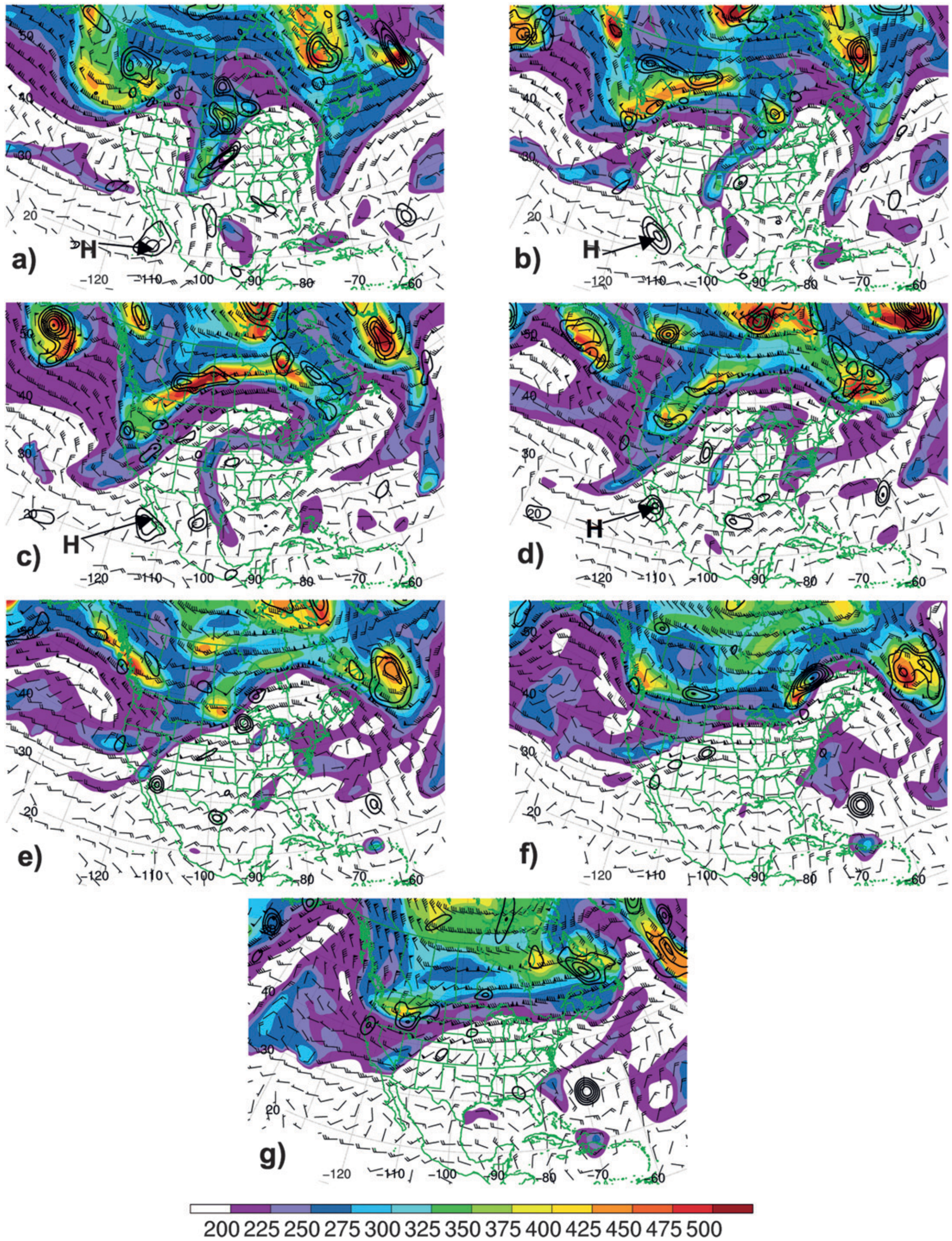


FIG. 12. As in Fig. 11, but every 24 h from (a) 1200 UTC 23 Aug through (g) 1200 UTC 29 Aug 1993 for Hurricane Hilary (H).

(Fig. 14a), moved west and then north with the storm (Figs. 14b–e) and helped the Marie remnants fight off the encroachment of, and interaction with, a small, but long-lived cyclonic anomaly on the DT located near 33°N, 124°W on Fig. 14a that broke off the southern end of the trough over the northern plains. The anticyclonic circulation eventually propagated east and away from the TC remnant by 0000 UTC 14 September (Fig. 14g) in advance of a very strong Pacific trough that advected the cyclonic DT anomaly northeastward (it is located over northern California in Fig. 14h). The digging trough also increased the winds over the Marie remnants, causing

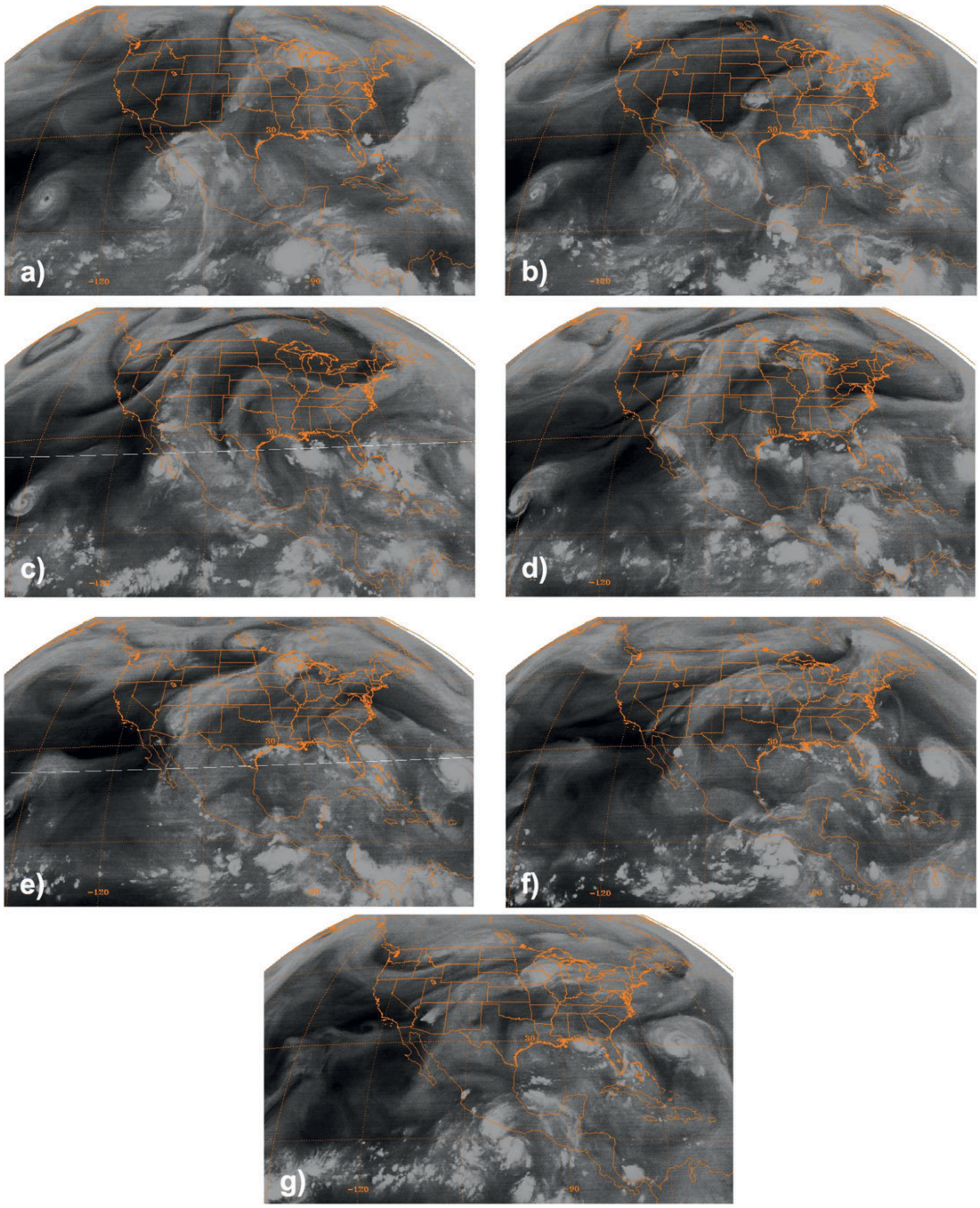


FIG. 13. *GOES-7* water vapor (~6.7 $\mu$m) satellite imagery every 24 h at ~1200 UTC from 23 to 29 Aug 1993 to match the maps in Fig. 12. [Images courtesy of the National Climatic Data Center (NCDC) GIBBS Web site at http://www.ncdc.noaa.gov/gibbs/.]

the vorticity signature to elongate and weaken below $4 \times 10^{-5}$ s$^{-1}$ as it became sheared out on the forward side of the trough.

## 5. Summary and future work

The eastern North Pacific is climatologically the most active basin for TC development, yet traditionally relatively little attention has been given to these systems because they rarely make landfall as major storms along the western coasts of Mexico and the United States. The present study has shown, however, that eastern Pacific TCs need not make landfall or even remain classified as tropical systems for their impact to be felt in the western United States. Using ERA-40 analyses, the NHC/TPC best track, and a high-resolution precipitation dataset,

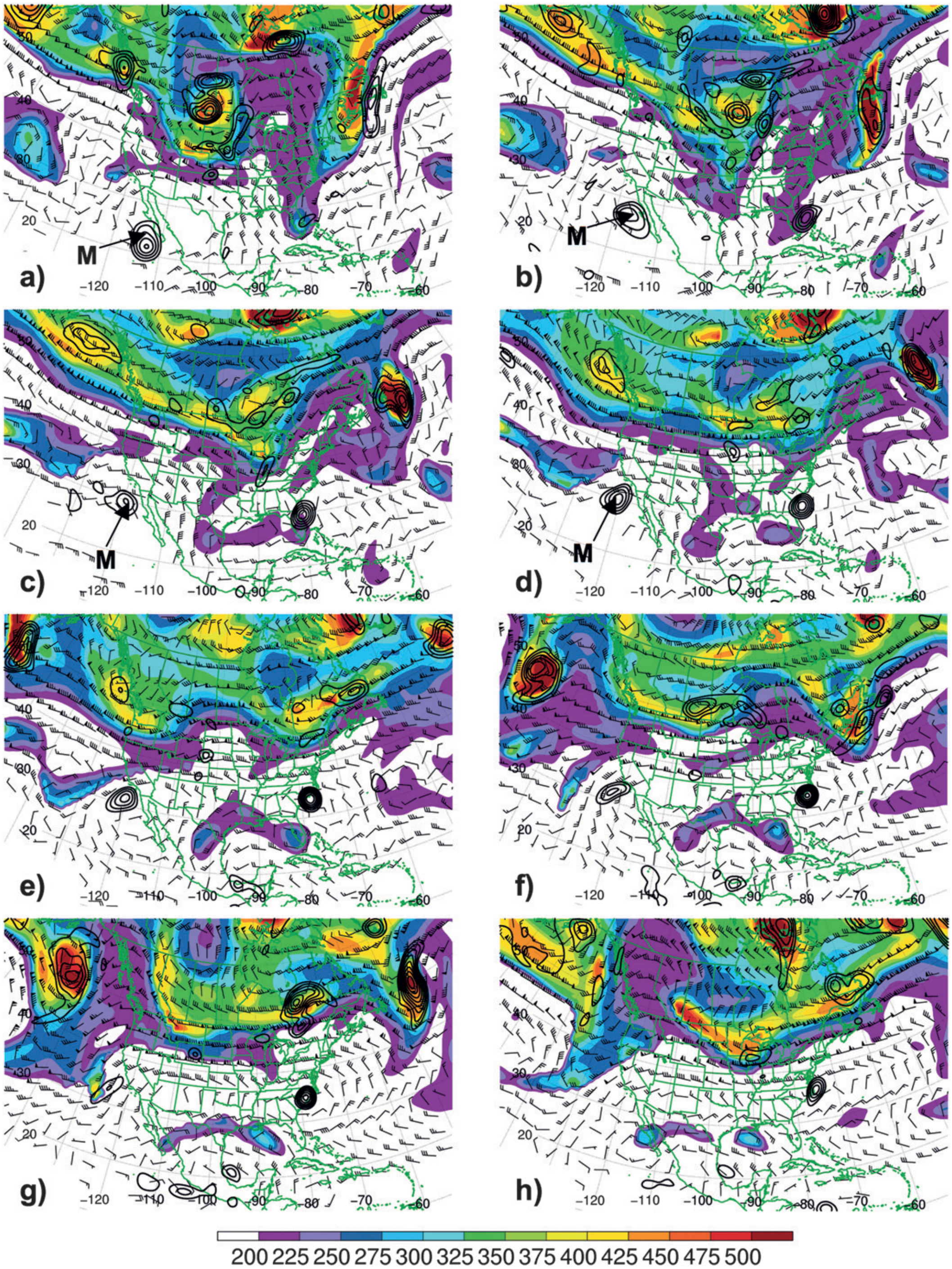


FIG. 14. As in Fig. 11, but every 24 h from (a) 0000 UTC 8 Sep through (h) 0000 UTC 15 Sep 1984 for Hurricane Marie (M).

35 eastern Pacific TCs and their remnants could be tracked into the southwest United States between 1958 and 2003, representing less than 10% of TC activity in the basin. The storms that affect the region are unique in that they form significantly closer to the Mexican coast than average, making them much more likely to acquire a northward component to their motion from the midlatitude troughs that begin to penetrate deep enough into the eastern Pacific during the month of September to cause the storms to recurve. Averaged over

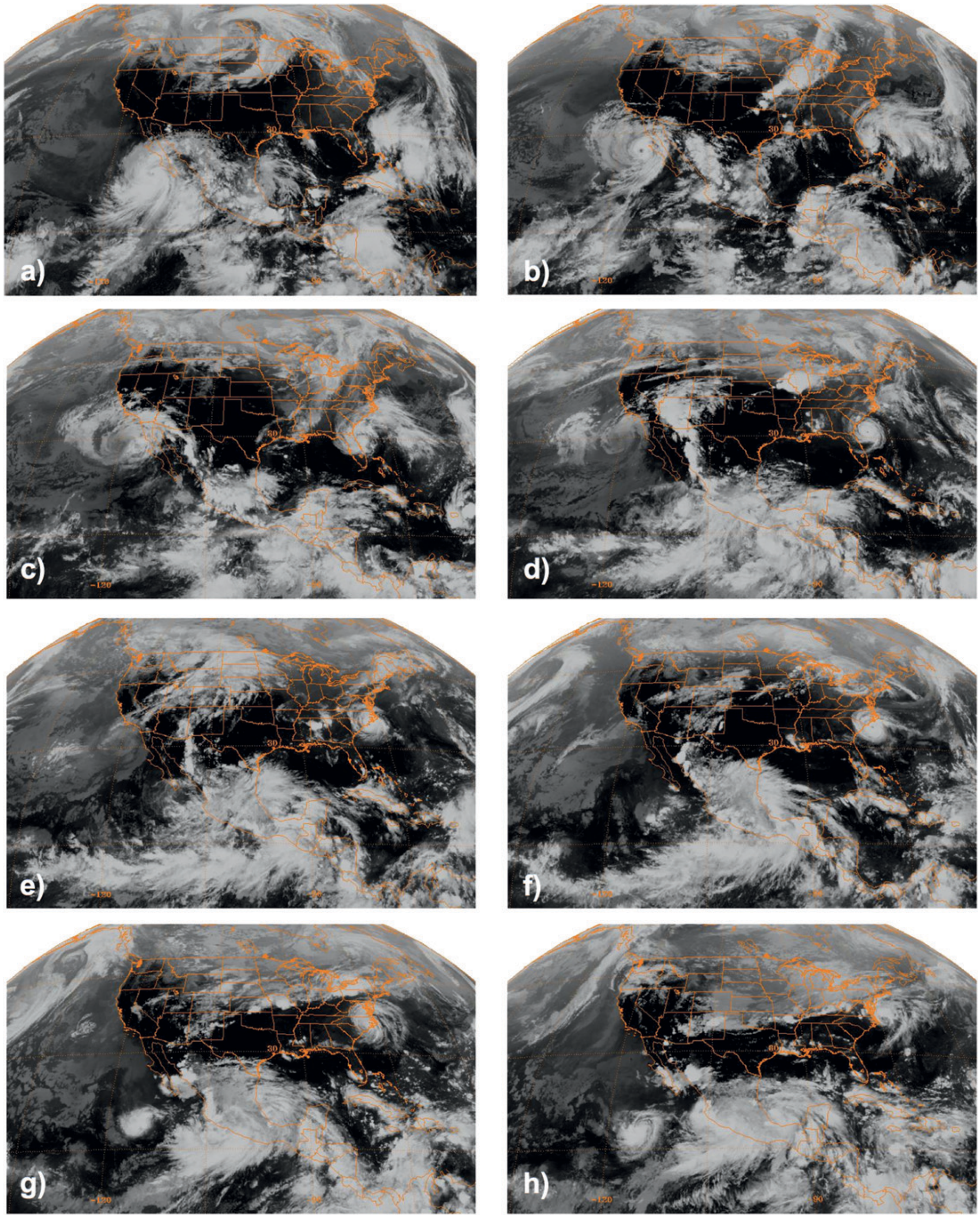


FIG. 15. As in Fig. 13, but from the *GOES-6* IR (~11 $\mu$m) channel every 24 h at ~0000 UTC from 8 to 15 Sep 1984.

all TC rainfall events, the contribution of TCs to the summer precipitation climatology of the monsoon region increases from less than 5% in central New Mexico to greater than 20% over extreme southern California. Individual storms can, however, account for upward of 95% of the summer rainfall experienced in the region and thus represent a significant water management and forecast challenge.

The distribution of rainfall in southwest U.S. TC events fell broadly into three categories: 1) a direct south to north track into southern California and Nevada, associated with a cutoff cyclone situated off the coast of California; 2) a distinct swath of heavy precipitation cutting northeastward from southwestern Arizona through northwestern New Mexico and into Colorado, as the TC remnants and tropical moisture were advected northeastward along the forward edge of a mobile midlatitude trough; and 3) a broad blanket of precipitation over the monsoon region with no distinct directional swaths and maxima tied to terrain features, generally not associated with a direct interaction with midlatitude features.

The avenues for future research involving TCs that bring rainfall to the southwest United States are myriad and several are currently under way. As noted above, the moisture and low-level vorticity associated with TC remnants can be tracked thousands of kilometers downstream over the continental United States. Analysis of these long-lived systems reveals a rich array of synoptic- and large-scale flow patterns associated with their introduction to, and interaction with, the midlatitudes. These interactions include significant amplification of the downstream flow pattern over the continental United States, becoming wrapped up in a developing midlatitude system, or remaining as a separate vorticity maximum and exhibiting the classic signatures of ET. Individual, in-depth case studies are currently underway exploring each of these situations and will be detailed in forthcoming manuscripts.

*Acknowledgments.* This project grew out of a graduate-level research class conducted by one of the authors (LB) at SUNY Albany during the fall of 2002. Class members who contributed to the beginnings of this work are Alicia Wasula, Kelly Lombardo, Brandon Smith, Susanna Hopsch, and Matthew Novak. We are indebted to David Vollaro for providing scripts to plot the best-track data and download the ERA-40 analyses from NCAR, and to Thomas Galarneau for help in downloading and processing the ERA-40 analyses. This work was partially supported by the Advanced Study Program at NCAR (KC) and National Science Foundation Grant ATM0553017 (LB).

## REFERENCES

Adams, D. K., and A. C. Comrie, 1997: The North American monsoon. *Bull. Amer. Meteor. Soc.,* **78,** 2197–2213.

Adams, J. L., and D. J. Stensrud, 2007: Impact of tropical easterly waves on the North American monsoon. *J. Climate,* **20,** 1219–1238.

Anderson, B. T., J. O. Roads, S.-C. Chen, and H.-M. H. Juang, 2000a: Regional simulation of the low-level monsoon winds over the Gulf of California and southwestern United States. *J. Geophys. Res.,* **105,** 17 955–17 969.

——, ——, and ——, 2000b: Large-scale forcing of summertime monsoon surges over the Gulf of California and the southwestern United States. *J. Geophys. Res.,* **105,** 24 455–24 467.

Archambault, H. M., L. F. Bosart, D. Keyser, and A. Aiyyer, 2008: Influence of large-scale flow regimes on cool-season precipitation in the northeastern United States. *Mon. Wea. Rev.,* **136,** 2945–2963.

Atallah, E., L. F. Bosart, and A. R. Aiyyer, 2007: Precipitation distribution associated with landfalling tropical cyclones over the eastern United States. *Mon. Wea. Rev.,* **135,** 2185–2206.

Badan-Dangon, A., C. E. Dorman, M. A. Merrifield, and C. D. Winant, 1991: The lower atmosphere over the Gulf of California. *J. Geophys. Res.,* **96,** 16 877–16 896.

Berbery, E. H., and M. S. Fox-Rabinovitz, 2003: Multiscale diagnosis of the North American monsoon system using a variable-resolution GCM. *J. Climate,* **16,** 1929–1947.

Bordoni, S., and B. Stevens, 2006: Principal component analysis of the summertime winds over the Gulf of California: A gulf surge index. *Mon. Wea. Rev.,* **134,** 3395–3414.

——, P. E. Ciesielski, R. H. Johnson, B. D. McNoldy, and B. Stevens, 2004: The low-level circulation of the North American monsoon as revealed by QuikSCAT. *J. Geophys. Res.,* **31,** L10109, doi:10.1029/2004GL020009.

Brenner, I. S., 1974: A surge of maritime tropical air—Gulf of California to the southwestern United States. *Mon. Wea. Rev.,* **102,** 375–389.

Bryson, R., and W. P. Lowry, 1955: Synoptic climatology of the Arizona summer precipitation singularity. *Bull. Amer. Meteor. Soc.,* **36,** 329–339.

Carleton, A. M., 1986: Synoptic-dynamic character of "bursts" and "breaks" in the southwest U.S. summer precipitation singularity. *J. Climatol.,* **6,** 605–623.

——, 1987: Summer circulation climate of the American Southwest, 1945–1984. *Ann. Assoc. Amer. Geogr.,* **77,** 619–634.

Chan, J. C. L., and W. M. Gray, 1982: Tropical cyclone movement and surrounding flow relationships. *Mon. Wea. Rev.,* **110,** 1354–1374.

Corbosiero, K. L., and J. Molinari, 2002: The effects of vertical wind shear on the distribution of convection in tropical cyclones. *Mon. Wea. Rev.,* **130,** 2110–2123.

Daida, S. K., and G. M. Barnes, 2003: Hurricane Paine (1986) grazes the high terrain of the Baja California peninsula. *Wea. Forecasting,* **18,** 981–990.

Dickinson, M., L. Bosart, K. Corbosiero, S. Hopsch, K. Lombardo, M. Novak, B. Smith, and A. Wasula, 2004: The extratropical transitions of eastern Pacific Hurricane Lester (1992) and Atlantic Hurricane Andrew (1992): A comparison. Preprints, *26th Conf. on Hurricanes and Tropical Meteorology,* Miami, FL, Amer. Meteor. Soc., 17D.2. [Available online at http://ams.confex.com/ams/pdfpapers/75685.pdf.]

Douglas, M. W., and J. C. Leal, 2003: Summertime surges over the Gulf of California: Aspects of their climatology, mean structure, and evolution from radiosonde, NCEP reanalysis, and rainfall data. *Wea. Forecasting,* **18,** 55–74.

——, R. A. Maddox, K. Howard, and S. Reyes, 1993: The Mexican monsoon. *J. Climate,* **6,** 1665–1677.

Englehart, P. J., and A. V. Douglas, 2001: The role of eastern North Pacific tropical storms in the rainfall climatology of western Mexico. *Int. J. Climatol.,* **21,** 1357–1370.

Farfán, L. M., 2004: Regional observations during the landfall of Tropical Cyclone Juliette (2001) in Baja California, Mexico. *Mon. Wea. Rev.,* **132,** 1575–1589.

——, 2005: Development of convective systems over Baja California during Tropical Cyclone Linda (2003). *Wea. Forecasting,* **20,** 801–811.

——, and J. A. Zehnder, 2001: An analysis of the landfall of Hurricane Nora (1997). *Mon. Wea. Rev.,* **129,** 2073–2088.

——, and M. Cortez, 2005: An observational and modeling study of the landfall of Hurricane Marty (2003) in Baja California, Mexico. *Mon. Wea. Rev.,* **133,** 2069–2090.

Frank, W. M., and E. A. Ritchie, 1999: Effects of environmental flow upon tropical cyclone structure. *Mon. Wea. Rev.,* **127,** 2044–2061.

——, and ——, 2001: Effects of vertical wind shear on hurricane intensity and structure. *Mon. Wea. Rev.,* **129,** 2249–2269.

Fuller, R. D., and D. J. Stensrud, 2000: The relationship between tropical easterly waves and surges over the Gulf of California during the North American monsoon. *Mon. Wea. Rev.,* **128,** 2983–2989.

Gochis, D. J., W. J. Shuttleworth, and Z.-L. Yang, 2003: Hydrometeorological response of the modeled North American monsoon to convective parameterization. *J. Hydrometeor.,* **4,** 235–250.

Gray, W. M., 1968: Global view of the origin of tropical disturbances and storms. *Mon. Wea. Rev.,* **96,** 669–700.

Gutzler, D. S., E. A. Ritchie, A. V. Douglas, and M. D. Lewis, 2006: Interannual variability of near-coastal eastern Pacific tropical cyclones. Preprints, *27th Conf. on Hurricanes and Tropical Meteorology,* Monterey, CA, Amer. Meteor. Soc., P2.6. [Available online at http://ams.confex.com/ams/pdfpapers/108952.pdf.]

Hales, J. E., Jr., 1972: Surges of maritime tropical air northward over the Gulf of California. *Mon. Wea. Rev.,* **100,** 298–306.

Higgins, R. W., and W. Shi, 2005: Relationships between Gulf of California moisture surges and tropical cyclones in the eastern Pacific basin. *J. Climate,* **18,** 4601–4620.

——, Y. Yao, and X. L. Wang, 1997: Influence of the North American monsoon system on the U.S. summer precipitation regime. *J. Climate,* **10,** 2600–2622.

——, and Coauthors, 2003: Progress in pan-American CLIVAR research: The North American monsoon system. *Atmósfera,* **16,** 29–65.

——, W. Shi, and C. Hain, 2004: Relationships between Gulf of California moisture surges and precipitation in the southwestern United States. *J. Climate,* **17,** 2983–2997.

Jáuregui, E., 2003: Climatology of landfalling hurricanes and tropical storms in Mexico. *Atmósfera,* **16,** 193–204.

Kalnay, E., and Coauthors, 1996: The NCEP/NCAR 40-Year Reanalysis Project. *Bull. Amer. Meteor. Soc.,* **77,** 437–471.

Kistler, R., and Coauthors, 2001: The NCEP–NCAR 50–Year Reanalysis: Monthly means CD–ROM and documentation. *Bull. Amer. Meteor. Soc.,* **82,** 247–267.

Larson, J., Y. Zhou, and R. W. Higgins, 2005: Characteristics of landfalling tropical cyclones in the United States and Mexico: Climatology and interannual variability. *J. Climate,* **18,** 1247–1262.

Li, C., and M. Yanai, 1996: The onset and interannual variability of the Asian summer monsoon in relation to land–sea thermal contrast. *J. Climate,* **9,** 358–375.

Magaña, V., J. A. Amador, and S. Medina, 1999: The midsummer drought over Mexico and central America. *J. Climate,* **12,** 1577–1588.

Manning, D., and R. E. Hart, 2007: Evolution of North Atlantic ERA40 tropical cyclone representation. *Geophys. Res. Lett.,* **34,** L05705, doi:10.1029/2006GL028266.

Molinari, J., D. Vollaro, S. Skubis, and M. Dickinson, 2000: Origins and mechanisms of eastern Pacific tropical cyclogenesis: A case study. *Mon. Wea. Rev.,* **128,** 125–139.

Morehouse, B. J., R. H. Carter, and T. W. Sprouse, 2000: The implications of sustained drought for transboundary water management in Nogales, Arizona and Nogales, Sonora. *Nat. Resour. J.,* **40,** 783–817.

Morgan, M. C., and J. W. Nielson-Gammon, 1998: Using tropopause maps to diagnose midlatitude weather systems. *Mon. Wea. Rev.,* **126,** 2555–2579.

Rasmussen, E. M., 1967: Atmospheric water vapor transport and the water balance of North America. Part I: Characteristics of the water vapor flux field. *Mon. Wea. Rev.,* **95,** 403–427.

Ritchie, E. A., and D. Szenasi, 2006: The impact of tropical cyclone remnants on the rainfall of the North American southwest region. Preprints, *27th Conf. on Hurricanes and Tropical Meteorology,* Monterey, CA, Amer. Meteor. Soc., 13D.4. [Available online at http://ams.confex.com/ams/pdfpapers/137924.pdf.]

Rodgers, E. B., R. F. Adler, and H. F. Pierce, 2000: Contribution of tropical cyclones to the North Pacific climatological rainfall as observed from satellites. *J. Appl. Meteor.,* **39,** 1658–1678.

Schmitz, T. J., and S. L. Mullen, 1996: Water vapor transport associated with the summertime North American monsoon as depicted by ECMWF analyses. *J. Climate,* **9,** 1621–1634.

Serra, C. S., 1971: Hurricanes and tropical storms of the west coast of Mexico. *Mon. Wea. Rev.,* **99,** 302–308.

Stensrud, D. J., R. L. Gall, and M. K. Nordquist, 1997: Surges over the Gulf of California during the Mexican monsoon. *Mon. Wea. Rev.,* **125,** 417–437.

Thorncroft, C. D., B. J. Hoskins, and M. E. McIntyre, 1993: Two paradigms of baroclinic-wave life-cycle behaviour. *Quart. J. Roy. Meteor. Soc.,* **119,** 17–55.

Uppala, S. M., and Coauthors, 2005: The ERA-40 reanalysis. *Quart. J. Roy. Meteor. Soc.,* **131,** 2961–3012.

Vera, C., and Coauthors, 2006: Toward a unified view of the American monsoon system. *J. Climate,* **19,** 4977–5000.

Zehr, R. M., 1992: Tropical cyclogenesis in the western North Pacific. NOAA Tech. Rep. NESDIS 61, 181 pp.